Environmental Science & Technology

pubs.acs.org/est

Article

Absolute and Fast Removal of Viruses and Bacteria from Water by Spraying-Assembled Carbon-Nanotube Membranes

Dongwei Ma, Hengyi Li, Zixun Meng, Chenxu Zhang, Jiemei Zhou, Jianzhong Xia, and Yong Wang*

Cite This: *Environ. Sci. Technol.* 2021, 55, 15206−15214

Read Online

ACCESS | Metrics & More | Article Recommendations | Supporting Information

ABSTRACT: Membrane separation is able to efficiently remove pathogens like bacteria and viruses from water based on size exclusion. However, absolute and fast removal of pathogens requires highly permeable but selective membranes. Herein, we report the preparation of such advanced membranes using carbon nanotubes (CNTs) as one-dimensional building blocks. We first disperse CNTs with the help of an amphiphilic block copolymer, poly(2-dimethylaminoethyl methacrylate)-*block*-polystyrene (PDMAEMA-*b*-PS, abbreviated as BCP). The PS blocks adsorb on the surface of CNTs via the $\pi-\pi$ interaction, while the PDMAEMA blocks are solvated, thus forming homogeneous and stable CNT dispersions. We then spray the CNT dispersions on porous substrates, producing composite membranes with assembled CNT layers as the selective layers. We demonstrate that the optimized membrane shows 100% rejection to phage viruses and bacteria (*Escherichia coli*) while giving a water permeance up to ∼3300 L m^{-2} h^{-1} bar^{-1}. The performance of the resultant BCP/CNT membrane outperforms that of state-of-the-art membranes and commercial membranes. The BCP/CNT membrane can be used for multiple runs and regenerated by water rinsing. Membrane modules assembled from large-area membrane sheets sustain the capability of absolute and fast removal of viruses and bacteria.

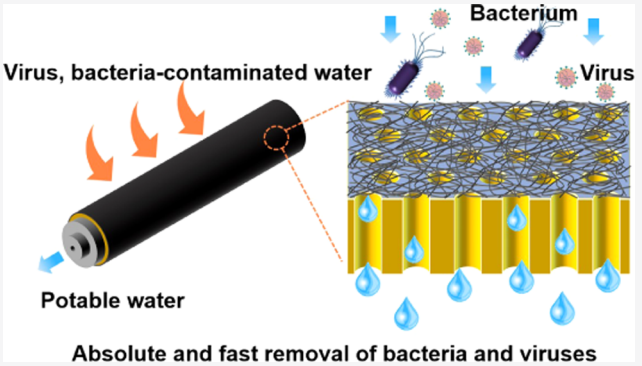

KEYWORDS: *carbon nanotube, spray coating, block copolymer, bacterium, virus*

1. INTRODUCTION

The reliable and affordable access to clean water is one of the biggest worldwide challenges in our age.[1] Currently, around four billion people are facing severe water shortage at least 1 month a year,[2] while the global water consumption is expected to increase by 20−30% to the year 2050 because of the population growth and industrialization.[3] One main reason for the shortage of potable water is the presence of waterborne microbes such as pathogenic bacteria and viruses in natural and recycled water.[4] An extreme case is that SARS-CoV-2 causing the worldwide pandemic of COVID-19[5−7] has recently been detected alive in municipal water and wastewater.[8,9] To purify the microbe-contaminated water, disinfection approaches including boiling, UV irradiation, and chlorination are extensively utilized.[10] However, it is challenging for many of these disinfection technologies to kill all of the microbes in water, and thus the absolute removal of microbes cannot be realized. Propagation of the surviving bacteria and viruses will soon make thus-disinfected water impotable again. Moreover, these microbe-killing technologies leave dead bodies of bacteria and viruses in water, which may cause severe pyretogenic issues when used as injection water.[11] In comparison, membrane separation, based on the size-sieving effect, can physically remove all microbes larger than the membrane pores, thus preventing the leakage of microorganisms into the treated effluent. In addition, this filtration-based disinfection process requires no heating, produces no wastes, and is highly energy-efficient and environmentally benign.[12,13]

Viruses are one of the most intractable pathogens in drinking water and their small sizes, typically ranging from 20 to 120 nm,[14,15] make them difficult to be completely removed from water with fast rates using conventional membranes. The key to solving this issue is to use membranes with a narrow pore-size distribution, high porosity, and low water resistance, which completely retain viruses while allowing fast transport of water. A promising strategy to prepare such selective but fast membranes is to assemble one-dimensional (1D) nanostructures on the surface of macroporous substrates.[16,17] Tightly assembling these 1D nanostructures produces high-density, interconnected fine gaps, which can serve as a sieving gate for

Received: July 14, 2021
Revised: October 20, 2021
Accepted: October 21, 2021
Published: October 29, 2021

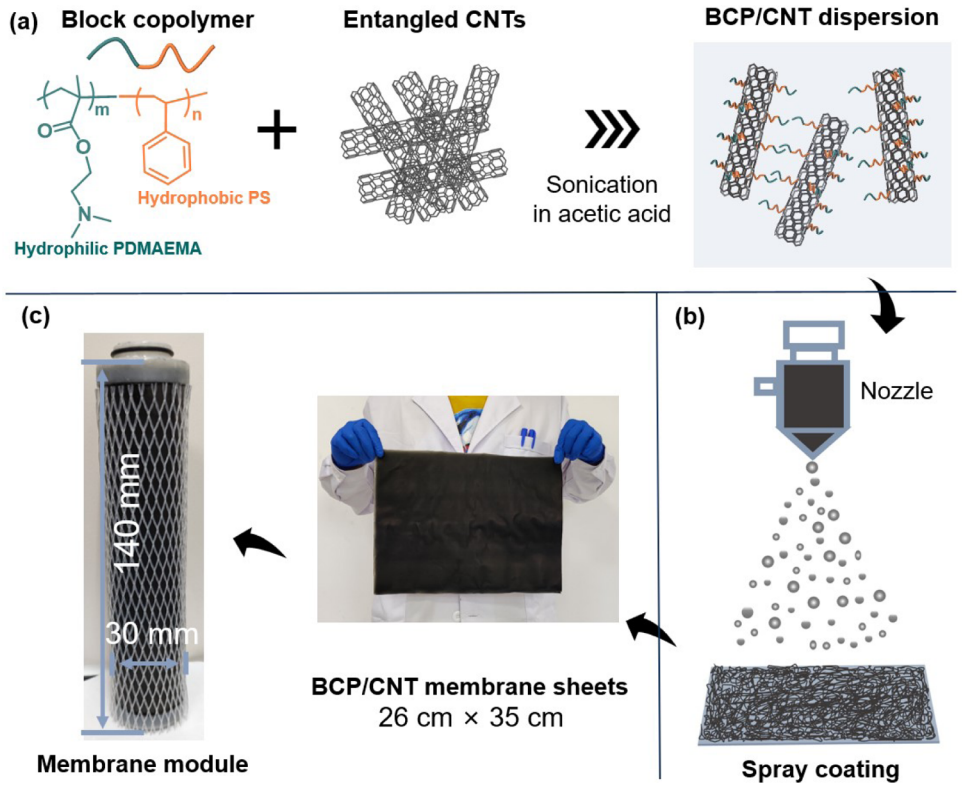

Figure 1. Preparation of the BCP/CNT membrane module for viruses and bacteria removal. (a) Stabilization of entangled CNTs by BCPs under sonication. (b) Schematic diagram of the spray coating process to produce BCP/CNT membrane sheets. (c) Membrane module assembled from a few sheets of BCP/CNT membranes.

efficient separations. A variety of 1D nanostructures including inorganic nanowires and polymeric nanofibers have been used in this regard, and carbon nanotubes (CNTs) are attracting considerable interest in the virtues of their superior mechanical and chemical stabilities and easy availability of tubes with designable lengths and diameters.[18−20] Jin and co-workers[21−23] reported pioneering work in this area. They performed a series of treatments to disperse single-walled CNTs, and the CNT dispersions were vacuum-filtered on porous substrates followed by the removal of the substrate to obtain free-standing CNT membranes. Thus-obtained CNT membranes with the thickness of tens of nanometers transferred on porous ceramic substrates can effectively separate both micrometer- and nanometer-sized water-in-oil emulsions with remarkable fluxes. Additionally, the membranes assembled from either single-walled or multiwalled CNTs[24−26] were used as ultrafiltration substrates with tunable pore sizes and surface functionalities, on which the interfacial polymerization was conducted to synthesize polyamide composite membranes. Thanks to the high porosity and devisable surface functionalities of the assembled CNTs, the composite membranes supported by the CNT substrates exhibit enhanced water permeances at no or little expense of salt rejections in reverse osmosis (RO) and forward osmosis (FO).[27]

Significantly, an essential prerequisite to preparing CNT membranes is the good dispersion of CNTs in solvents. CNTs are typically present in the form of entangled and non-dispersible aggregates, and enormous efforts are required to disperse and stabilize CNTs in liquids before processing them into the desired structures.[25,26,28] To this end, surface functionalization is usually required to generate active groups on the surface of CNTs to enhance the repulsion between tubes. Furthermore, surfactants are used under extensive sonication to disperse CNTs to obtain homogeneous and stable CNT dispersions.[29,30] Unavoidably, a large portion of surfactants remain in the membranes, which may gradually leak into the permeated water and cause safety and health issues.[31,32] Alternatively, amphiphilic block copolymers (BCPs) having both hydrophobic and hydrophilic chains are recognized as a new class of dispersants to disperse CNTs in polar solvents.[33−35] There is no need to remove the BCPs, which serve as glues to enhance the stability of CNT membranes.[34] These BCPs have large molecular weights and cannot be dissolved in water, avoiding the potential leaking issue. In addition, the hydrophilic chains of BCPs are present on the surface of the CNT membranes, thus significantly enhancing the water wettability and consequently water permeability.

The fast and effective deposition of CNTs is another issue that needs to be solved in fabricating CNT-based membranes. Vacuum fitration[36,37] is the widely used wet approach in the lab to prepare assembled CNT membranes. Elimelech et al. reported CNT-based microfilters to remove waterborne pathogens completely via an electrochemical process.[38,39] Nevertheless, the CNT-based microfilters, prepared by vacuum filtration, with tens of micrometers in thickness have high water transport resistance.[40] In addition, vacuum filtration works in the batch-by-batch mode, suffering from the limited productivity and membrane area. In contrast, spray operates continuously and is able to form uniform coating layers on the surface of dense or porous substrates with arbitrary sizes. Spraying CNT dispersions on porous substrates leads to the continuous formation of assembled CNT layers with flexibly tunable thicknesses on the substrates, enabling the large-scale

https://doi.org/10.1021/acs.est.1c04644
Environ. Sci. Technol. 2021, 55, 15206−15214

production of CNT membranes with adjustable permeabilities and selectivities.

In this work, to prepare high-flux membranes able to completely remove bacteria and viruses from water, as shown in Figure 1, we use multiwalled CNTs as 1D building blocks and disperse them in acetic acid with the help of amphiphilic BCPs, poly(2-dimethylaminoethyl methacrylate)-*block*-polystyrene (PDMAEMA-*b*-PS). The BCP-stabilized CNT (BCP/CNT) dispersions are then spray-coated on macroporous substrates, producing fast but selective membranes. BCPs act as dispersants to disperse and stabilize CNTs before spraying coating and act as glue after spraying to integrate the individual CNTs to form a tight porous network on the substrate surface. The thickness of the CNT layer and the separation performance can be precisely tuned by varying the sprayed volumes of BCP/CNT dispersions. The effective pore size of the membranes can be well below 100 nm and a water permeance as high as 2580-4400 L m^{-2} h^{-1} bar^{-1} can be obtained. We demonstrate that the resultant BCP/CNT membranes can absolutely remove bacteria and phage viruses from water. Moreover, the BCP/CNT membranes exhibit good reusability and can be regenerated by simple water rinsing. Membrane modules assembled from the spray-coated BCP/CNT membrane sheets also show a high water flux, implying their industrial application in water purification. This work demonstrates that spray coating of stabilized BCP/CNT dispersions is an effective and up-scalable strategy to prepare advanced membranes suitable for the absolute removal of microbes from water.

2. MATERIALS AND METHODS

2.1. Materials. BCP with a polydispersity index (PDI) of 1.26 was synthesized from our reported method.[41] BCP has a molecular weight (M_n) of 80.8 kDa and the weight ratio of PDMAEMA was 25.7%. Multiwalled CNTs with an outer diameter of 10−20 nm, a length of 10−30 μm, and purity of >98% were used as purchased from XFNANO Materials Technology Co., Ltd. Polyethersulfone (PES) support with an average pore size of 0.45 μm was purchased from Haining Xindongfang Technology Co. Ltd. A commercial polysulfone (PSF) membrane with a molecular weight cutoff of 500 kDa was provided by Beijing OriginWater Membrane Technology Co., Ltd. All analytical reagents, including acetic acid (HAc, ≥99.0%), *N*-methyl-2-pyrrolidone (NMP, ≥99.0%), and ethanol (≥99.7%) were purchased from local suppliers and used without further purification, if not specially mentioned. Monodispersed gold colloidal nanoparticles with a diameter of 50 nm were purchased from British Biocell International. Bovine serum albumin (BSA, 98.0%, 66 kDa) and tablets of phosphate-buffered saline (PBS) were obtained from MP Biomedicals, LLC. The PBS solution with a pH of 7.4 was prepared by dissolving one tablet of PBS in 100 mL of deionized (DI) water. DI water obtained from a local supplier (conductivity: <5 $\mu S \cdot cm^{-1}$) was used in all experiments.

2.2. Preparation of BCP/CNT Dispersions. A total of 50 mg of CNTs was added into 100 g of HAc and sonicated for 30 min at a power of 600 W. Then, 25 mg of BCP was added into the CNT suspension and sonicated for another 2 h at a power of 200 W. BCP/CNT dispersions with varied weight ratios of BCPs to CNTs were obtained in the same way. Nascent BCP/CNT dispersions were centrifuged at a low speed of 3000 rpm for 5 min to remove the large CNT aggregates. Well-dispersed supernatants of BCP/CNT were suctioned to use.

2.3. Preparation of BCP/CNT Membranes and Membrane Modules. A spray machine (SEV-300EDN, Suzhou Second Automatic Equipment Co., Ltd) was placed in a fume hood. The setup of the spray machine was the same as our previous work.[42] Typically, PES supports with a size of 15 × 10 cm^2 (or 26 × 35 cm^2) were clamped on the heating plate of the spray setup. Afterward, the BCP/CNT dispersion was poured in the spray reservoir and then atomized under the compressed air pressure, and uniformly sprayed onto the PES substrate. The spray nozzle scanned the PES support repeatedly until the PES support was completely covered by the BCP/CNT nanofibers. Finally, a uniform and defect-free BCP/CNT composite membrane could be obtained after the stacking of BCP/CNT nanofibers. A few sheets of BCP/CNT membranes with large lateral sizes were assembled to customize a membrane module (Figures 1c and 4a).

2.4. Characterizations. A UV−vis spectrometer (Nanodrop 2000C, Thermo scientific) was used to detect the dispersity and stability of the BCP/CNT dispersions. The BCP/CNT dispersion was diluted 30 times by ethanol, and a specific spectrum at ∼230 nm was recorded. The BCP/CNT dispersion was diluted 30 times by ethanol to characterize the particle-size distribution of samples by the dynamic light scattering (DLS, Zetasizer Nano ZS 90, Malvern, England). The CNT and BCP/CNT dispersions were dropped on the silicon substrates to perform Raman spectroscopy using a Raman spectrometer (HR800, Labram) using an excitation laser with a wavelength of 532 nm. The surfaces and cross-sectional morphologies of the BCP/CNT membranes were characterized by a field-emission scanning electron microscope (FE-SEM, Hitachi S4800) at an accelerating voltage of 5 kV and a working distance of ∼9 mm. The BCP/CNT membranes were quick-frozen by soaking in liquid nitrogen and cut by scissors for the cross-sectional observation. All samples were sputter-coated with gold for 20 s to prevent charging effects during SEM image capture. The thicknesses of the BCP/CNT layers were determined according to the cross-sectional SEM images. The pore-size distributions of the BCP/CNT membranes were characterized by utilizing a capillary flow porometer (iPore-1500AEX-Clamp). The CNT and BCP/CNT dispersions were spray-coated on the silicon substrates to carry out water contact angle (WCA) tests for analyzing the surface wettability by a contact angle goniometer (DropMeter A-100, Maist). The surface wettability of the PES substrate and the BCP/CNT membrane was characterized in the same way.

2.5. Filtration Tests and Antifouling Performance. The separation performances of the BCP/CNT membranes were evaluated using a customized dead-end apparatus with an effective permeation area of 12.8 cm^2. Circular membrane coupons with a diameter of 47 mm were cut from the flat-sheet BCP/CNT membranes to carry out filtration tests. The evaluation of the water flux was performed at a pressure of 1 bar. Prior to the assessment of the water flux, precompaction of the BCP/CNT membranes at 1.5 bar was performed to ensure a stable flux. The BCP/CNT membrane module was tested by a cross-flow apparatus. The gold colloid was used to assess the rejection ability of the BCP/CNT membranes. The gold colloid concentrations in feed, permeation, and retentate were detected using a UV−vis feature absorption spectrometer at ∼520 nm. The rejection rate of gold nanoparticles was calculated according to eq 1

https://doi.org/10.1021/acs.est.1c04644
Environ. Sci. Technol. 2021, 55, 15206−15214

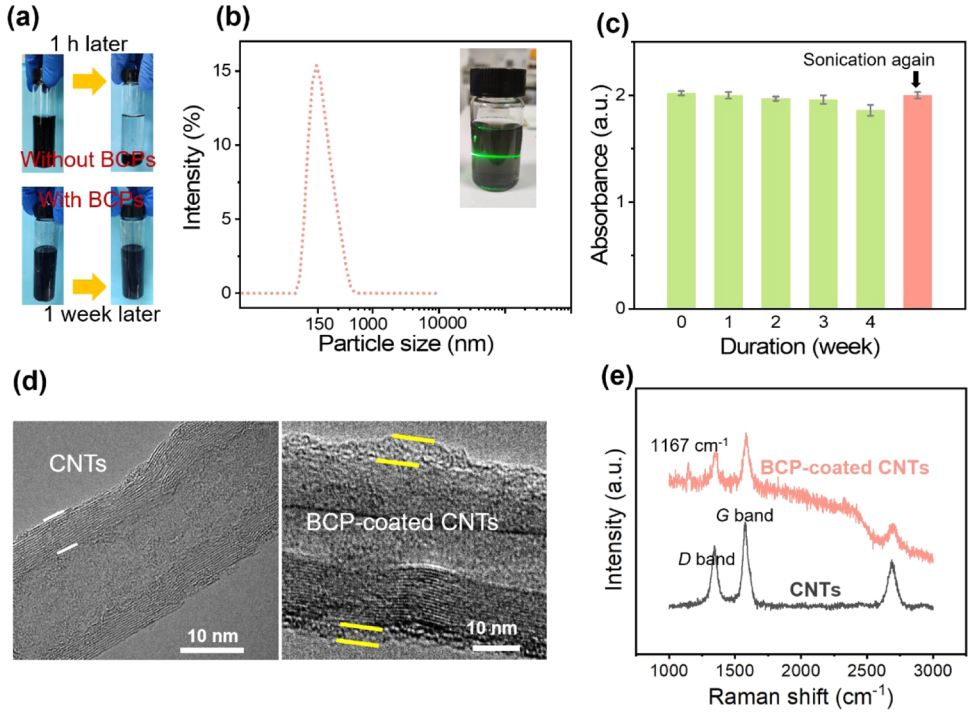

Figure 2. Stability of the BCP/CNT dispersion and morphologies of the BCP-coated CNTs. (a) CNT dispersions in HAc with and without BCPs. (b) DLS characterization of the 1:2 BCP/CNT dispersion, the inset in (b) shows the picture showing the Tyndall effect of the diluted 1:2 BCP/CNT dispersion. (c) Stability of the 1:2 BCP/CNT dispersion monitored by UV−vis spectrometry. (d) Transmission electron microscopy (TEM) images of pure CNTs and the BCP-coated CNTs. (e) Raman spectra of pristine CNTs and BCP-coated CNTs.

$$R = 100\% \times (1 - C_p/C_f) \quad (1)$$

where C_p and C_f (mg L^{-1}) are gold nanoparticle concentrations in the permeation and the feed solutions, respectively.

The antifouling performances of the BCP/CNT composite membranes were investigated using BSA as a model biofoulant. In a typical static protein adsorption experiment, a piece of BCP/CNT membrane with a diameter of 47 mm was floating on 5 mL of BSA solutions with a concentration of 1 g mL^{-1} (pH = 7.4) at room temperature for 12 h. The amount of BSA adsorption was calculated according to eq 2

$$q = V \times (C_0 - C_t)/A \quad (2)$$

where q (g cm^{-2}) is the adsorption capacity for 12 h, V (mL) is the volume of the protein solution, C_0 (g mL^{-1}) is the initial BSA concentration, C_t (g mL^{-1}) is the BSA concentration after adsorption for 12 h, and A (cm^{-2}) is the surface area of the BCP/CNT membrane.

2.6. Virus and Bacterial Removal Tests. The removal of viruses and bacteria by membrane module was carried out at the Tsinghua University. Sterile saline water with an *E. coli* suspension (~6×10^6 organisms per mL) and a phage virus suspension (~5×10^6 organisms per mL) was utilized to assess the removal ability of the BCP/CNT membranes. The *E. coli* suspension or the phage virus suspension was subjected to a filtration process through the BCP/CNT membrane module. After filtration, bacterial and viral cultures were carried out to visually present the removal efficiency of the BCP/CNT membranes. The feed and filtrate of the *E. coli* suspension diluted 1×10^4 times were cultured and incubated at ~37 °C for 24 h. The feed and filtrate of the phage virus suspension diluted 1×10^5 times were cultured and incubated at ~25 °C overnight. The unfiltered suspensions of *E. coli* and phage virus showed the growth of bacterial and viral colonies, whereas this growth was invisible in the filtered solutions.

3. RESULTS AND DISCUSSION

3.1. Characterization of BCP/CNT Dispersions. The poor dispersity of CNTs has constrained their processibility in membrane fabrication. To utilize CNTs facilely, the first step is to help CNTs to be well dispersed in proper solvents. The BCP was used to stabilize CNTs in this work. As shown in Figure 2a, pure CNTs were hard to disperse in the polar solvent of HAc even by strong sonication for a long duration. Because of the strong van der Waals force between CNTs,[36] CNTs were susceptible to aggregate together and were totally precipitated in HAc after standing for 0.5−1 h. In contrast, CNTs could be readily dispersed in HAc at different mass ratios of BCPs to CNTs (1:2, 1:1, and 2:1) and remained stable even after being kept undisturbed for 1 week at room temperature (Figures 2a and S1b,c,f,g). However, with increasing mass ratios of BCPs to CNTs, redundant BCPs formed micelles embedded between CNTs (Figure S2), which block the interstices between CNTs and increase water transport resistance (also see discussions in Figure S5). Lower dosages were also explored, but they did not produce sufficiently stable dispersion. As shown in Figure S1a,d, CNT dispersions produced at BCP/CNT = 1:3 were partially precipitated after about 1 day of standing and prone to jam the nozzle during spray coating, and CNTs were precipitated at the bottom of the bottle after 1 week of standing (Figure S1e). Therefore, a moderate mass ratio of BCP/CNT, 1:2, was used in our following study to prepare homogeneous CNT dispersions. As shown in the inset of Figure 2b, a strong Tyndall effect of the diluted BCP/CNT dispersion also confirmed the good dispersibility of CNTs in HAc. The DLS

https://doi.org/10.1021/acs.est.1c04644
Environ. Sci. Technol. 2021, 55, 15206−15214

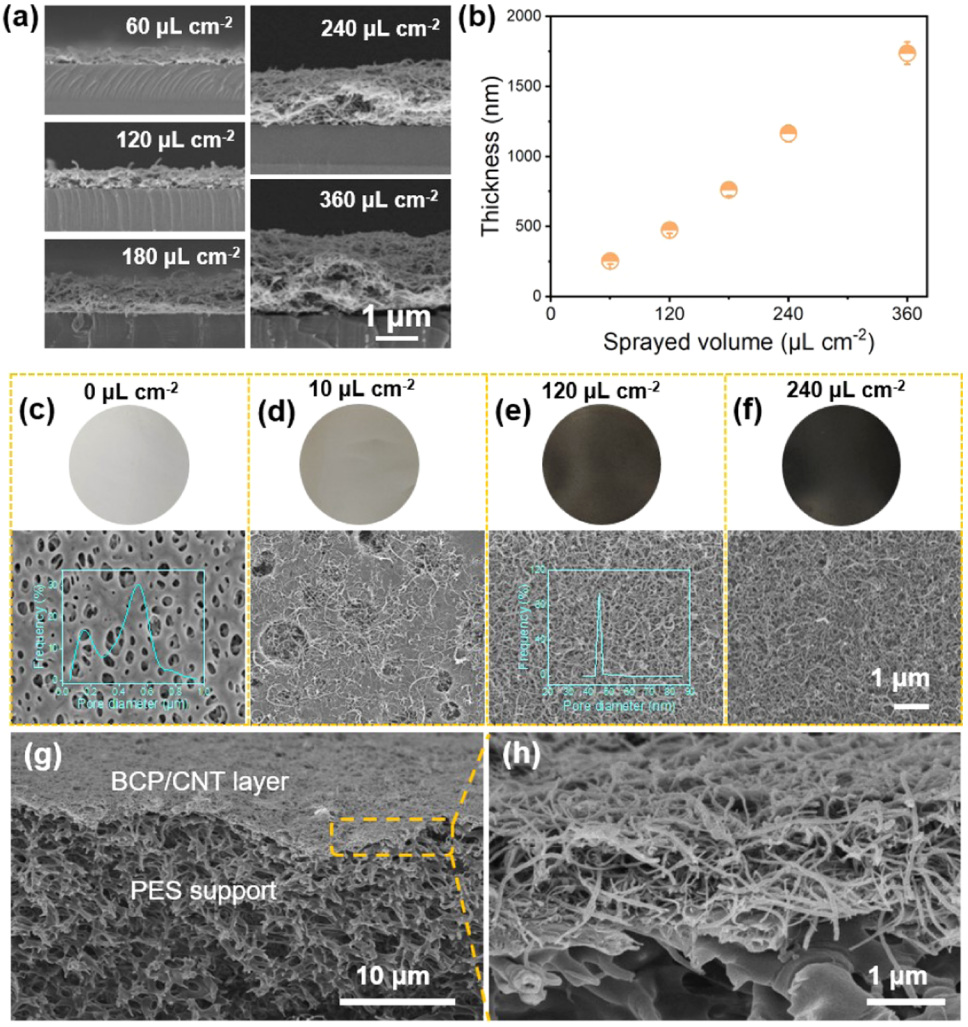

Figure 3. Morphology characterizations of BCP/CNT membranes. (a) Thickness variation and cross-sectional morphologies of the BCP/CNT layers on the silicon substrates with different sprayed volumes. SEM images in (a) have the same magnification, and the scale bar corresponds to 1 μm. (b) Thickness variation of the BCP/CNT layers on the silicon substrates with different sprayed volumes. (c–f) Digital and SEM images of the BCP/CNT membranes with different sprayed volumes having the same magnification, and the scale bar corresponds to 1 μm as presented in (f). Insets in (c) and (e) show the pore-size distributions of the corresponding membranes. (g, h) Cross-sectional SEM images of the BCP/CNT membrane with a sprayed volume of 240 μL cm^{-2}.

characterization showed a narrow size distribution of the BCP/CNT dispersion. In addition, the concentration variation of the BCP/CNT dispersion was monitored by UV–vis spectrometry, as shown in Figure 2c. The concentration of the BCP/CNT dispersion was almost the same even after being preserved at room temperature for 3 weeks. A slight drop of ~8% occurred in the 4th week, indicating the precipitation of a small number of CNTs. However, the precipitated CNTs could be redispersed well after short ultrasonication. These observations clearly exhibited the good dispersity and stability of the BCP/CNT dispersions in HAc.

TEM, SEM, and Raman characterizations were utilized to explore the role of BCP in the CNT dispersion. As shown in Figure 2d, the pristine CNTs consist of ~16 laminar graphite layers with a total thickness of ~7 nm and the average diameter of CNTs is about 22 nm, according to the SEM and TEM images. In the presence of BCPs, the core/shell composite containing inside crystalline CNTs and a thin amorphous BCP coating layer can be clearly observed. As shown in Figure S3, the average diameter of the BCP-coated CNTs is enlarged to 39 nm. It can be deduced that the thickness of the BCP coating layer is ~8.5 nm. Moreover, as shown in Figure 2e, pristine CNTs have a specific D band at 1342 cm^{-1} and a G band at 1577 cm^{-1} in the Raman spectrum, corresponding to the defect and graphitic phases of CNTs, respectively. In comparison, the Raman spectrum of BCP-coated CNTs displayed a new absorbance at ~1167 cm^{-1}, corresponding to the characteristic band of BCP. In addition, it can be found that the surface hydrophilicity of CNTs was changed after being coated by BCPs. As presented in the insets of Figure S3a,b, the WCA of pristine CNTs is 147.2°. In stark contrast, the WCA of the BCP-coated CNTs is reduced to 84.1°. The enhanced hydrophilicity of the BCP-coated CNTs should be originated from the hydrophilic PDMAEMA blocks of the BCP.

3.2. Thickness Tunability of BCP/CNT Membranes during Spray Coating. According to the Hagen–Poiseuille (H–P) equation, the water flux of an ultrafiltration membrane is inverse to the thickness of its selective layer.[43] Therefore, it is an efficient way to improve the water flux by reducing the thickness of the selective layer. Spray coating was utilized to build the BCP/CNT thin films as the separation layers. To

https://doi.org/10.1021/acs.est.1c04644
Environ. Sci. Technol. 2021, 55, 15206–15214

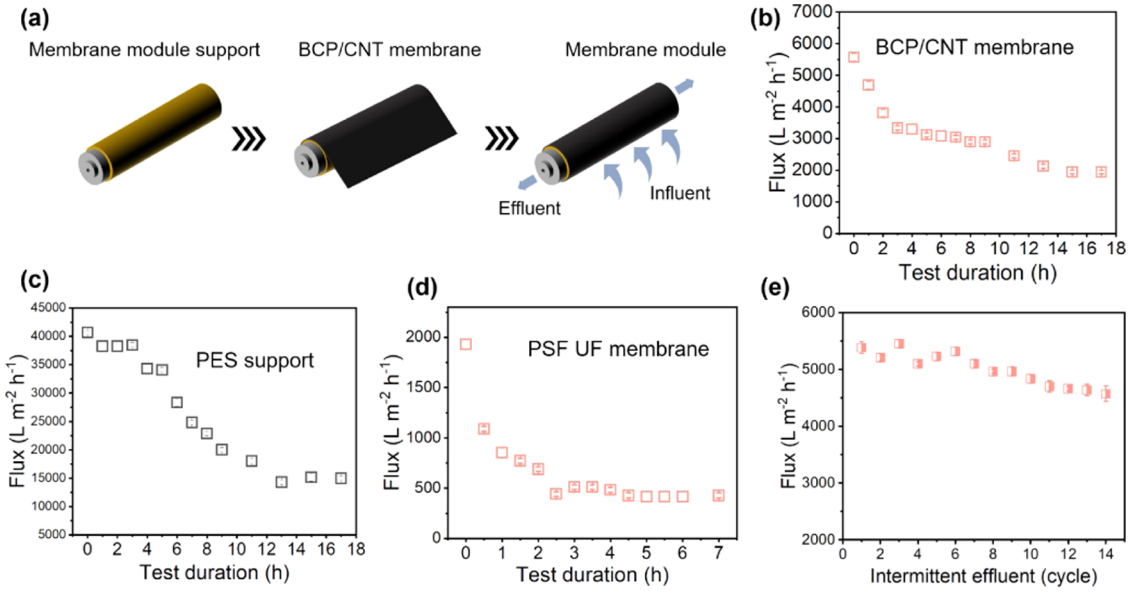

Figure 4. Comparison of the membrane module assembled from different types of membrane sheets. (a) Schematic diagram of the membrane module assemble process. (b–d) Water flux variation of the membrane modules with test time at the pressure of 2 bar. (e) Simulated intermittent effluents of the BCP/CNT membranes.

clearly observe the thickness variation of the BCP/CNT layers with the sprayed volumes of dispersions, we sprayed different volumes of the BCP/CNT dispersions on the surface of silicon substrates. As shown in Figure 3a,b, the thicknesses of the BCP/CNT layers were almost linearly increased from 254 to 1737 nm with the sprayed volume increased from 60 to 360 μL cm^{-2}, which should be attributed to the good dispersibility of the BCP/CNT dispersions and excellent controllability of spray coating. These results demonstrated the capability of spray coating to readily tune the thickness of the selective layer, allowing the tunability to membrane performances.

We then sprayed the BCP/CNT dispersions on macroporous PES substrates to prepare BCP/CNT composite membranes with the assembled BCP-coated CNTs as the selective layers. As shown in Figures 3c–f and S4a–c, with the sprayed volumes of the BCP/CNT dispersions increased from 0 to 360 μL cm^{-2}, the color of the top surface of membranes changes from milky white to black. With a low sprayed volume of 10 μL cm^{-2}, the macropores of PES substrates cannot be fully covered by the BCP-coated CNTs (Figure 3d), while increasing the sprayed volume to 60 μL cm^{-2} is able to form an integrated layer of densely stacked and overlapped BCP-coated CNTs atop the PES support without the presence of any defects or uncovered macropores (Figure S4a). With the dispersion sprayed volume increased from 60 to 120, 180, 240, and 360 μL cm^{-2}, the surface of the BCP/CNT membranes shows no obvious difference (Figures 3e,f, and S4b,c). The bilayered structure composed of the BCP-coated CNT layer and the PES support can be clearly observed in Figure 3g,h. We then used a capillary flow porometer to examine the pore-size distributions of the obtained BCP/CNT membranes. As shown in the inset of Figure 3c, the PES supports with a nominal pore size of 450 nm exhibit a bimodal pore-size distribution widely scattered between ~50 and 950 nm. In stark contrast, the BCP/CNT composite membranes consistently present sharp pore-size distributions with a largely narrowed sieving size (inset in Figures 3e and S4d). In detail, the pore-size distributions are centered at 54, 44, and 29 nm with the sprayed volumes of 60, 120, and 180 μL cm^{-2}, respectively. The reduction of pore size arises from the tight stack and interlacement of multilayered BCP/CNT nanofibers.

3.3. Separation Performances of BCP/CNT Membranes. Membrane modules were designed to evaluate the performances of the BCP/CNT membranes in practical applications. As shown in the schematic illustration of Figure 4a, a few sheets of the BCP/CNT membranes with large lateral sizes were assembled to customize a membrane module (Figure 1c). This membrane module with a dimension of a 14 cm length and a 3 cm outer diameter was designed. As shown in Figure 4b, although the water flux of the membrane module drops significantly with a continuous test for 17 h at a pressure of 2 bar, its flux remains stable around 2000 L m^{-2} h^{-1}, which is much higher than commercial membranes (in the range of 20–135 L m^{-2} h^{-1} bar^{-1}).[44] The loose structure of the BCP/CNT layer, high porosity of the composite membrane, and the compaction of the PES support are the main reasons for the sharp flux decrease of the membrane module. As shown in Figure 4c, the water flux of the PES support dramatically decreased from ~40 000 to ~15 000 L m^{-2} h^{-1} because of the compaction of the PES support itself. As shown in Figure 4d, a commercial PSF UF membrane was also subjected to this test. The water flux of the PSF UF membranes was decreased sharply from ~2000 to ~500 L m^{-2} h^{-1} after 3 h. Clearly, our BCP/CNT membranes exhibit superior stability and much higher water permeance than the commercial PSF UF membranes. Moreover, we simulated the intermittent pattern of domestic direct drinking fountains. As shown in Figure 4e, 2.5 L of purified water can be obtained in 2.5 min and a total of 35 L of purified water can be obtained after 14 cycles, which meets the drinking water consumption in most families.

3.4. Removal of Bacteria and Viruses by BCP/CNT Membranes. The removal of pathogens such as bacteria and viruses in drinking water is essential for human health. Two common microbes in drinking water are *E. coli* and phage viruses, which are responsible for many waterborne diseases. As shown in Figure 5a,d, *E. coli* with an average size of ~0.5

https://doi.org/10.1021/acs.est.1c04644
Environ. Sci. Technol. 2021, 55, 15206–15214

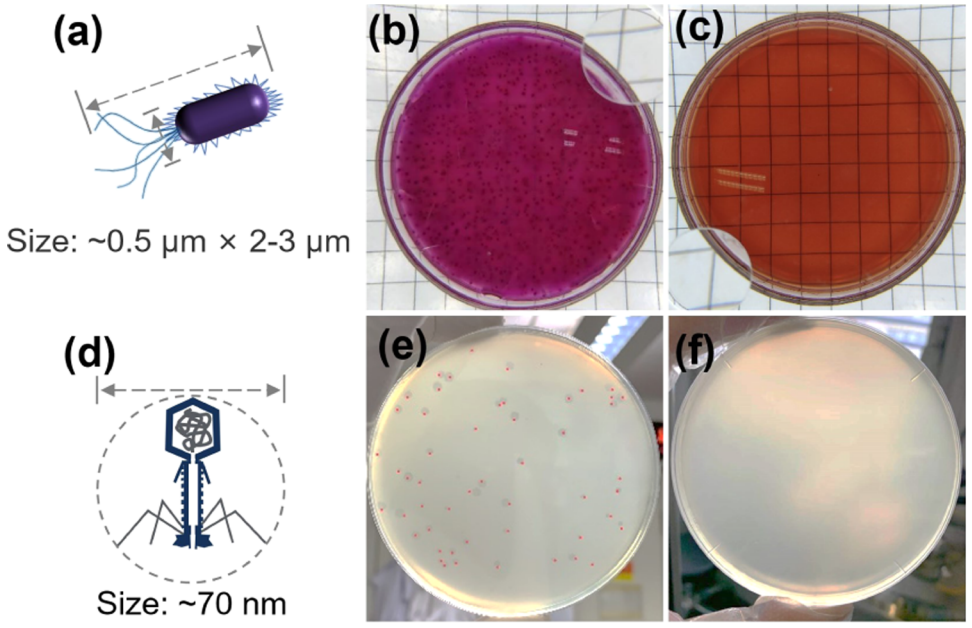

Figure 5. Bacterial and phage viral removal by the BCP/CNT membrane module. (a) Schematic diagram of *E. coli*. Photographs of the *E. coli* colonies on agar plates inoculated with feed (b) and the filtrate (c) through the BCP/CNT membrane module. (d) Schematic diagram of the phage virus. Photographs of the phage virus colonies on agar plates inoculated with feed (e) and the filtrate (f) through the BCP/CNT membrane module.

μm × 2−3 μm as well as a phage virus with an average size of ∼70 nm was chosen to serve as the model microbes in water. We used the membrane module to filter the suspension containing *E. coli* (∼6 × 10^6 organisms per mL) or enveloped phage viruses (∼5 × 10^6 organisms per mL), and then examined the possible presence of these microbes in the permeated water. As shown in Figure 5b,c,e,f, the unfiltered suspensions of *E. coli* and phage virus showed the growth of bacterial and viral colonies, whereas no *E. coli* and phage virus colonies can be detected in the agar plates of the permeated water, which implies that both *E. coli* and phage viruses were 100% retained by the membrane modules. Therefore, we conclude that our BCP/CNT membranes have the capability to absolutely remove the bacteria and viruses from water for human consumption. The removal mechanism of viruses and bacteria is predominantly by size exclusion. As-prepared BCP/CNT membranes possess numerous nanoscale pores, and they can work as a sieve to repulse large-sized viruses and bacteria while allowing the fast permeation of water under the applied transmembrane pressures. By this filtration process, the pathogens are successfully removed from water, thus generating sterile water. The SARS-CoV-2 virus has an average size of ∼120 nm,[7,45] much bigger than the phage virus. As we have clearly demonstrated that our BCP/CNT membrane completely rejects the phage viruses, we believe that this membrane is also able to 100% remove all of the SARS-CoV-2 viruses possibly existing in water at a fast rate.

■ ASSOCIATED CONTENT

Supporting Information

The Supporting Information is available free of charge at https://pubs.acs.org/doi/10.1021/acs.est.1c04644.

Digital images of BCP/CNT dispersions, SEM and TEM images of BCP/CNT nanofibers, pore-size distributions of BCP/CNT membranes, ultrafiltration performance of the BCP/CNT membrane, multiple filtration test, membrane performance comparison, backwash and abrasion resistance, and digital images of a free-standing CNT film (PDF)

■ AUTHOR INFORMATION

Corresponding Author

Yong Wang − *State Key Laboratory of Materials-Oriented Chemical Engineering, College of Chemical Engineering, Nanjing Tech University, Nanjing 211816 Jiangsu, P. R. China;* orcid.org/0000-0002-8653-514X; Email: yongwang@njtech.edu.cn

Authors

Dongwei Ma − *State Key Laboratory of Materials-Oriented Chemical Engineering, College of Chemical Engineering, Nanjing Tech University, Nanjing 211816 Jiangsu, P. R. China*

Hengyi Li − *Beijing OriginWater Membrane Technology Co., Ltd., Beijing 101407, P. R. China*

Zixun Meng − *State Key Laboratory of Materials-Oriented Chemical Engineering, College of Chemical Engineering, Nanjing Tech University, Nanjing 211816 Jiangsu, P. R. China*

Chenxu Zhang − *State Key Laboratory of Materials-Oriented Chemical Engineering, College of Chemical Engineering, Nanjing Tech University, Nanjing 211816 Jiangsu, P. R. China*

Jiemei Zhou − *State Key Laboratory of Materials-Oriented Chemical Engineering, College of Chemical Engineering, Nanjing Tech University, Nanjing 211816 Jiangsu, P. R. China*

Jianzhong Xia − *Institute for Advanced Study, Shenzhen University, Shenzen 518060 Guangdong, P. R. China;* orcid.org/0000-0003-1563-9563

Complete contact information is available at: https://pubs.acs.org/10.1021/acs.est.1c04644

https://doi.org/10.1021/acs.est.1c04644
Environ. Sci. Technol. 2021, 55, 15206−15214

Notes

The authors declare no competing financial interest.

■ ACKNOWLEDGMENTS

The authors gratefully acknowledge financial support from the National Science Fund for Distinguished Young Scholars (21825803) and the Project of Priority Academic Program Development of Jiangsu Higher Education Institutions (PAPD).

■ REFERENCES

(1) Tortajada, C.; Rensburg, P. V. Drink More Recycled Wastewater. *Nature* **2020**, *577*, 26−28.
(2) Mekonnen, M. M.; Hoekstra, A. Y. Four Billion People Facing Severe Water Scarcity. *Sci. Adv.* **2016**, *2*, No. e1500323.
(3) Ercin, A. E.; Hoekstra, A. Y. Water Footprint Scenarios for 2050: A Global Analysis. *Environ. Int.* **2014**, *64*, 71−82.
(4) Bethencourt, V. Virus Stalls Genzyme Plant. *Nat. Biotechnol.* **2009**, *27*, 681.
(5) Wong, J. P.; Damania, B. SARS-CoV-2 Dependence on Host Pathways. *Science* **2021**, *371*, 884−885.
(6) Simmons, B. A.; Ray, R.; Yang, H.; Gallagher, K. P. China Can Help Solve the Debt and Environmental Crises. *Science* **2021**, *371*, 468−470.
(7) Kumar, M.; Thakur, A. K.; Mazumder, P.; Kuroda, K.; Mohapatra, S.; Rinklebe, J.; Ramanathan, A.; Cetecioglu, Z.; Jain, S.; Tyagi, V. K.; Gikas, P.; Chakraborty, S.; Tahmidul Islam, M.; Ahmad, A.; Shah, A. V.; Patel, A. K.; Watanabe, T.; Vithanage, M.; Bibby, K.; Kitajima, M.; Bhattacharya, P. Frontier Review on the Propensity and Repercussion of SARS-CoV-2 Migration to Aquatic Environment. *J. Hazard. Mater. Lett.* **2020**, *1*, No. 100001.
(8) Liu, D.; Thompson, J. R.; Carducci, A.; Bi, X. Potential Secondary Transmission of SARS-CoV-2 via Wastewater. *Sci. Total Environ.* **2020**, *749*, No. 142358.
(9) Sherchan, S. P.; Shahin, S.; Ward, L. M.; Tandukar, S.; Aw, T. G.; Schmitz, B.; Ahmed, W.; Kitajima, M. First Detection of SARS-CoV-2 RNA in Wastewater in North America: A Study in Louisiana, USA. *Sci. Total Environ.* **2020**, *743*, No. 140621.
(10) Gall, A. M.; Mariñas, B. J.; Lu, Y.; Shisler, J. L. Waterborne Viruses: A Barrier to Safe Drinking Water. *PLoS Pathog.* **2015**, *11*, No. e1004867.
(11) Kuo, D.; Liu, M.; Kumar, K. R. S.; Hamaguchi, K.; Gan, K. P.; Sakamoto, T.; Ogawa, T.; Kato, R.; Miyamoto, N.; Nada, H.; Kimura, M.; Henmi, M.; Katayama, H.; Kato, T. High Virus Removal by Self-Organized Nanostructured 2D Liquid-Crystalline Smectic Membranes for Water Treatment. *Small* **2020**, *16*, No. 2001721.
(12) Otaki, M.; Yano, K.; Ohgaki, S. Virus Removal in a Membrane Separation Process. *Water Sci. Technol.* **1998**, *37*, 107−116.
(13) Gustafsson, O.; Manukyan, L.; Mihranyan, A. High-Performance Virus Removal Filter Paper for Drinking Water Purification. *Global Challenges* **2018**, *2*, No. 1800031.
(14) Shannon, M. A.; Bohn, P. W.; Elimelech, M.; Georgiadis, J. G.; Mariñas, B. J.; Mayes, A. M. Science and Technology for Water Purification in the Coming Decades. *Nature* **2008**, *452*, 301−310.
(15) Pendergast, M. M.; Hoek, E. M. V. A Review of Water Treatment Membrane Nanotechnologies. *Energy Environ. Sci.* **2011**, *4*, 1946−1971.
(16) Srivastava, A.; Srivastava, O. N.; Talapatra, S.; Vajtai, R.; Ajayan, P. M. Carbon Nanotube Filters. *Nat. Mater.* **2004**, *3*, 610−614.
(17) Brady-Estévez, A. S.; Kang, S.; Elimelech, M. A Single-Walled-Carbon-Nanotube Filter for Removal of Viral and Bacterial Pathogens. *Small* **2008**, *4*, 481−484.
(18) Kukovecz, Á.; Smajda, R.; Kónya, Z.; Kiricsi, I. Controlling the Pore Diameter Distribution of Multi-Wall Carbon Nanotube Buckypapers. *Carbon* **2007**, *45*, 1696−1698.
(19) Whitby, R. L. D.; Fukuda, T.; Maekawa, T.; James, S. L.; Mikhalovsky, S. V. Geometric Control and Tuneable Pore Size Distribution of Buckypaper and Buckydiscs. *Carbon* **2008**, *46*, 949−956.
(20) Roy, K.; Mukherjee, A.; Maddela, N. R.; Chakraborty, S.; Shen, B.; Li, M.; Du, D.; Peng, Y.; Lu, F.; García Cruzatty, L. C. Outlook on the Bottleneck of Carbon Nanotube in Desalination and Membrane-Based Water Treatment—A Review. *J. Environ. Chem. Eng.* **2020**, *8*, No. 103572.
(21) Shi, Z.; Zhang, W.; Zhang, F.; Liu, X.; Wang, D.; Jin, J.; Jiang, L. Ultrafast Separation of Emulsified Oil/Water Mixtures by Ultrathin Free-Standing Single-Walled Carbon Nanotube Network Films. *Adv. Mater.* **2013**, *25*, 2422−2427.
(22) Zhu, Y.; Xie, W.; Gao, S.; Zhang, F.; Zhang, W.; Liu, Z.; Jin, J. Single-Walled Carbon Nanotube Film Supported Nanofiltration Membrane with a Nearly 10 nm Thick Polyamide Selective Layer for High-Flux and High-Rejection Desalination. *Small* **2016**, *12*, 5034−5041.
(23) Wang, Z.; Wang, Z.; Lin, S.; Jin, H.; Gao, S.; Zhu, Y.; Jin, J. Nanoparticle-Templated Nanofiltration Membranes for Ultrahigh Performance Desalination. *Nat. Commun.* **2018**, *9*, No. 2004.
(24) Wu, M.-B.; Lv, Y.; Yang, H.-C.; Liu, L.-F.; Zhang, X.; Xu, Z.-K. Thin Film Composite Membranes Combining Carbon Nanotube Intermediate Layer and Microfiltration Support for High Nanofiltration Performances. *J. Membr. Sci.* **2016**, *515*, 238−244.
(25) Huang, J.; Hu, Y.; Bai, Y.; He, Y.; Zhu, J. Novel Solar Membrane Distillation Enabled by a PDMS/CNT/PVDF Membrane with Localized Heating. *Desalination* **2020**, *489*, No. 114529.
(26) Shen, C.; Zhu, Y.; Xiao, X.; Xu, X.; Chen, X.; Xu, G. Economical Salt-Resistant Superhydrophobic Photothermal Membrane for Highly Efficient and Stable Solar Desalination. *ACS Appl. Mater. Interfaces* **2020**, *12*, 35142−35151.
(27) Zhou, Z. Y.; Hu, Y. X.; Boo, C.; Liu, Z. Y.; Li, J. Q.; Deng, L. Y.; An, X. C. High-Performance Thin-Film Composite Membrane with an Ultrathin Spray-Coated Carbon Nanotube Interlayer. *Environ. Sci. Technol. Lett.* **2018**, *5*, 243−248.
(28) Ihsanullah. Carbon Nanotube Membranes for Water Purification: Developments, Challenges, and Prospects for the Future. *Sep. Purif. Technol.* **2019**, *209*, 307−337.
(29) Liu, Y.; Su, Y.; Cao, J.; Guan, J.; Zhang, R.; He, M.; Fan, L.; Zhang, Q.; Jiang, Z. Antifouling, High-Flux Oil/Water Separation Carbon Nanotube Membranes by Polymer-Mediated Surface Charging and Hydrophilization. *J. Membr. Sci.* **2017**, *542*, 254−263.
(30) Liu, Y.; Gao, G.; Vecitis, C. D. Prospects of an Electroactive Carbon Nanotube Membrane toward Environmental Applications. *Acc. Chem. Res.* **2020**, *53*, 2892−2902.
(31) Geng, H.-Z.; Lee, D. S.; Kim, K. K.; Han, G. H.; Park, H. K.; Lee, Y. H. Absorption Spectroscopy of Surfactant-Dispersed Carbon Nanotube Film: Modulation of Electronic Structures. *Chem. Phys. Lett.* **2008**, *455*, 275−278.
(32) Angelikopoulos, P.; Bock, H. Directed Self-Assembly of Surfactants in Carbon Nanotube Materials. *J. Phys. Chem. B* **2008**, *112*, 13793−13801.
(33) Zou, J.; Liu, L.; Chen, H.; Khondaker, S. I.; McCullough, R. D.; Huo, Q.; Zhai, L. Dispersion of Pristine Carbon Nanotubes Using Conjugated Block Copolymers. *Adv. Mater.* **2008**, *20*, 2055−2060.
(34) Yao, X.; Li, J.; Wang, Z.; Kong, L.; Wang, Y. Highly Permeable and Robust Membranes Assembled from Block-Copolymer-Functionalized Carbon Nanotubes. *J. Membr. Sci.* **2015**, *493*, 224−231.
(35) Zhou, Y.; Firkowska-Boden, I.; Arras, M. M. L.; Jandt, K. D. Polystyrene Homopolymer Enhances Dispersion of MWCNTs Stabilized in Solution by a PS-*b*-P2VP Copolymer. *Langmuir* **2021**, *37*, 391−399.
(36) Sears, K.; Dumée, L.; Schütz, J.; She, M.; Huynh, C.; Hawkins, S.; Duke, M.; Gray, S. Recent Developments in Carbon Nanotube Membranes for Water Purification and Gas Separation. *Materials* **2010**, *3*, 127−149.
(37) Rashed, A. O.; Merenda, A.; Kondo, T.; Lima, M.; Razal, J.; Kong, L.; Huynh, C.; Dumée, L. F. Carbon Nanotube Membranes—Strategies and Challenges Towards Scalable Manufacturing and

https://doi.org/10.1021/acs.est.1c04644
Environ. Sci. Technol. 2021, 55, 15206−15214

Practical Separation Applications. *Sep. Purif. Technol.* **2021**, *257*, No. 117929.
(38) Brady-Estévez, A. S.; Schnoor, M. H.; Vecitis, C. D.; Saleh, N. B.; Elimelech, M. Multiwalled Carbon Nanotube Filter: Improving Viral Removal at Low Pressure. *Langmuir* **2010**, *26*, 14975−14982.
(39) Rahaman, M. S.; Vecitis, C. D.; Elimelech, M. Electrochemical Carbon-Nanotube Filter Performance toward Virus Removal and Inactivation in the Presence of Natural Organic Matter. *Environ. Sci. Technol.* **2012**, *46*, 1556−1564.
(40) Vecitis, C. D.; Schnoor, M. H.; Rahaman, M. S.; Schiffman, J. D.; Elimelech, M. Electrochemical Multiwalled Carbon Nanotube Filter for Viral and Bacterial Removal and Inactivation. *Environ. Sci. Technol.* **2011**, *45*, 3672−3679.
(41) Zhang, C.; Yin, C.; Wang, Y.; Zhou, J.; Wang, Y. Simultaneous Zwitterionization and Selective Swelling-Induced Pore Generation of Block Copolymers for Antifouling Ultrafiltration Membranes. *J. Membr. Sci.* **2020**, *599*, No. 117833.
(42) Ma, D.; Zhou, J.; Wang, Z.; Wang, Y. Block Copolymer Ultrafiltration Membranes by Spray Coating Coupled with Selective Swelling. *J. Membr. Sci.* **2020**, *598*, No. 117656.
(43) Norman; Epstein. On Tortuosity and the Tortuosity Factor in Flow and Diffusion through Porous Media. *Chem. Eng. Sci.* **1989**, *44*, 777−779.
(44) Shah, V.; Wang, B.; Li, K. Blending Modification to Porous Polyvinylidene Fluoride (PVDF) Membranes Prepared via Combined Crystallisation and Diffusion (CCD) Technique. *J. Membr. Sci.* **2021**, *618*, No. 118708.
(45) Palika, A.; Armanious, A.; Rahimi, A.; Medaglia, C.; Gasbarri, M.; Handschin, S.; Rossi, A.; Pohl, M. O.; Busnadiego, I.; Gübeli, C.; Anjanappa, R. B.; Bolisetty, S.; Peydayesh, M.; Stertz, S.; Hale, B. G.; Tapparel, C.; Stellacci, F.; Mezzenga, R. An Antiviral Trap Made of Protein Nanofibrils and Iron Oxyhydroxide Nanoparticles. *Nat. Nanotechnol.* **2021**, *16*, 918−925.

https://doi.org/10.1021/acs.est.1c04644
Environ. Sci. Technol. 2021, 55, 15206−15214